

Genetic Dissection of SLE: *SLE1* and *FAS* Impact Alternate Pathways Leading to Lymphoproliferative Autoimmunity

Xiaoyan Shi,¹ Chun Xie,¹ Desi Kreska,¹ James A. Richardson,² and Chandra Mohan¹

¹Simmons' Arthritis Research Center and the Center for Immunology, and the ²Department of Pathology, University of Texas Southwestern Medical School, Dallas, TX 75235

Abstract

Genetic dissection of lupus pathogenesis in the NZM2410 strain has recently revealed that *Sle1* is a potent locus that triggers the formation of IgG anti-histone/DNA antibodies, when expressed on the B6 background as a congenic interval. B6.*lpr* mice, in contrast, exhibit distinctly different cellular and serological phenotypes. Both strains, however, do not usually exhibit pathogenic autoantibodies, or succumb to lupus nephritis. In this study, we show that the epistatic interaction of *Sle1* (in particular, *Sle1/Sle1*) with *FAS*^{lpr} leads to massive lymphosplenomegaly (with elevated numbers of activated CD4 T cells, CD4⁻CD8⁻ double negative (DN) T cells, and B1a cells), high levels of IgG and IgM antinuclear (including anti-ssDNA, anti-dsDNA, and anti-histone/DNA), and antiglomerular autoantibodies, histological, and clinical evidence of glomerulonephritis, and >80% mortality by 5–6 mo of age. Whereas *FAS*^{lpr} functions as a recessive gene, *Sle1* exhibits a gene dosage effect. These studies indicate that *Sle1* and *FAS*^{lpr} must be impacting alternate pathways leading to lymphoproliferative autoimmunity.

Key words: lupus • genetics • apoptosis • ALPS • anti-DNA

Introduction

Lupus is a truly polygenic disease where several distinct genetic aberrations and pathogenic events collectively orchestrate antinuclear antibody (ANA)* mediated systemic end-organ damage (for a review, see references 1 and 2). In particular, *Sle1*, *Sle2*, and *Sle3* are three major lupus susceptibility loci in the NZM2410 murine lupus model (3). When introgressed onto the normal C57BL/6 (B6) background, the NZM2410 alleles of these loci lead to very different immunophenotypes (4–13). *Sle1* triggers the formation of anti-histone/DNA Abs that react poorly with naked dsDNA (7). *Sle2* effects generalized B cell hyperactivity, leading to an expansion of B1 cells, and increased serum polyclonal/polyreactive Ig (6, 8). In contrast, *Sle3* leads to reduced activation-induced T cell death (AICD), increased CD4:CD8 ratios, and low-grade antinuclear seroreactivity (9). Although none of these loci engender se-

vere glomerulonephritis in isolation, the epistatic interaction of these loci leads to high-titred anti-dsDNA ANAs, severe GN, and mortality (10, 13).

The B6.*Sle1* strain has a rather peculiar seroprofile, compared with most other lupus-prone strains. In the BWF1 and MRL/*lpr* lupus models, as well as in lupus patients, anti-histone/DNA ANAs appear early in disease, and precede the emergence of anti-dsDNA ANAs (14–16). In contrast, this transition to anti-dsDNA (and nephrophilic) ANAs does not routinely occur in the B6.*Sle1* strain. Thus, <30% of these mice progress to develop anti-dsDNA ANA (7). This phenotype is reminiscent of that seen in patients with drug-induced lupus, who also develop anti-histone/DNA ANAs, but not renal disease (17). These observations suggest that anti-histone/DNA ANAs may not be pathogenic. More interestingly, these studies lend credence to the notion that anti-histone/DNA B cells may be regulated differently from anti-dsDNA B cells. Although *Sle1* may be sufficient to breach tolerance of anti-histone/DNA B-cells, additional mechanisms may be in place to check the emergence and evolution of anti-dsDNA B cells, and any consequent pathology.

Since *Sle3* has the potential to augment anti-dsDNA production, in epistasis with *Sle1*, *Sle3* may be representative of loci that regulate tolerance of anti-dsDNA B cells.

Address for correspondence to Chandra Mohan, Simmons Arthritis Research Center, Dept. of Internal Medicine/Rheumatology, UT Southwestern Medical Center Mail Code 8884, Y8.204 5323 Harry Hines Boulevard, Dallas, TX 75390-8884. Phone: 214-648-9675; Fax: 214-648-7995; E-mail: Chandra.mohan@utsouthwestern.edu

*Abbreviations used in this paper: ANA, antinuclear antibody; AICD, activation-induced T cell death; ALPS, autoimmune lymphoproliferative syndrome; BUN, blood urea nitrogen; DN, double negative; PerC, peritoneal cavity.

Although the culprit gene(s) within the *Sle3* locus remains unknown, we already know that *Sle3* has the potential to impair AICD, leading to an accumulation of activated T and B cells, with increasing age (9). Indeed, in many respects these phenotypes parallel those seen in *FAS^{lpr/lpr}* mice. The *lpr* mutation of *FAS* also impairs activation-induced lymphocyte apoptosis, leading to an accumulation of activated lymphocytes, serum anti-dsDNA ANAs, and clinical autoimmunity on certain genetic backgrounds (18, 19).

Although loci such as *Sle1* may be critical in modulating immune tolerance of anti-histone/DNA B cells, the regulation of anti-dsDNA specificities (and hence the development of end-organ disease) may require additional checkpoints, such as those modulated by *Sle3* and *FAS*. In this study we test this hypothesis by generating B6.*Sle1*|*lpr* mice, bearing both *Sle1* and *FAS^{lpr/lpr}*. Interestingly, these mice have greatly elevated levels of nephrophilic, anti-dsDNA ANAs, prominent lymphadenopathy and splenomegaly, and accelerated mortality, compared with B6, B6.*Sle1*, and B6.*lpr* controls. These observations suggest that the more pathogenic specificities (such as anti-dsDNA and nephrophilic Abs) must have been effectively tolerized in B6.*Sle1* mice through *FAS/FASL*-dependent mechanisms. Thus, *Sle1* and *FAS* appear to be impacting two alternate, nonredundant, pathways leading to lymphoproliferative autoimmunity.

Materials and Methods

Mice. C57BL/6 (B6) mice were obtained from The Jackson Laboratory and subsequently bred in our animal colony. The derivation of B6 congenic mice bearing NZM2410 derived lupus-susceptibility intervals has been detailed previously (4). B6.*Sle1* (i.e., B6.*Sle1^{NZM/NZM}*) mice are C57BL/6 mice congenic homozygotes for a 37 centimorgan interval on murine chromosome 1, spanning the 95% confidence interval flanking *Sle1*, derived from NZM2410, with termini at *D1MIT101* and *D1MIT155*. The immunological phenotypes of this strain have been reported previously (7). B6 mice bearing homozygous *FAS^{lpr/lpr}* mutations were obtained from The Jackson Laboratory, and are referred to as B6.*lpr*, for simplicity (18). B6.*Sle1*|*lpr* mice expressing *Sle1* and *FAS^{lpr/lpr}*, both homozygously, were derived by breeding B6.*Sle1* with B6.*lpr* mice for two generations, and then selecting F2 progeny that were homozygous at both loci. In addition, where indicated, mice bearing single copies of these loci were also studied. Thus, B6.*Sle1^{+/-}*|*lpr* mice are homozygous for *FAS^{lpr}*, but heterozygous at *Sle1*. Likewise, B6.*Sle1*|*lpr^{+/-}* mice are homozygous at *Sle1*, but heterozygous for *FAS^{lpr}*. The primers used to identify the *Sle1* interval and *FAS^{lpr}* have been detailed previously (4, 7, 20). All mice used for this study were bred and housed in a specific pathogen free colony at UT Southwestern Medical Center Department of Animal Resources in Dallas, TX. Equal numbers of male and female mice were used for all experiments, and any observed sex differences are indicated.

Cell Preparation and Culture. Splenocytes were depleted of red blood cells using Tris Ammonium Chloride, and single-cell suspensions were prepared for culture or flow cytometric analysis (described below). LN cells were obtained from the inguinal sites, and crushed to obtain single cell suspensions, for FACS[®]

analysis. Peritoneal cavity (PerC) cells were obtained by flushing the peritoneal cavities with fresh media. For the in vitro ANA production assays, red cell-depleted splenocytes were cultured (10^6 cells per well) with or without LPS (20 ug/ml; Sigma-Aldrich) at 37°C. Supernatants were harvested 5 d after culture, diluted 1:2, and assayed for total IgG or IgG ANAs by ELISA, as described below.

Flow Cytometric Analysis and Antibodies. FACS[®] was performed as described previously (6–10). In brief, cells were first blocked with staining medium (PBS, 5% horse serum, 0.05% azide) containing 10% normal rabbit serum. Cells were then stained on ice with optimal amounts of FITC, phycoerythrin, or biotin-conjugated primary Abs diluted in staining medium for 30 min. The following dye- or biotin-coupled Abs were obtained from BD PharMingen: CD4 (RM4–5); CD5 (53–7.3); CD8 (Ly–2); CD23 (B3B4); CD24 (M1/69); CD25 (7D4); CD43 (S7); CD44 (IM7); CD45R/B220 (RA3–6B2); CD62L (MEL14); CD69 (H1.2F3); CD80/B7–1 (16–10A1); CD86/B7–2 (GL1); and used at pretitrated dilutions. After two washes, the biotin-conjugated Abs were revealed using streptavidin-Tricolor (Caltag), or streptavidin-Quantum Red (Sigma-Aldrich). Cell staining was analyzed using a FACScan[™] (Becton Dickinson). Dead cells were excluded on the basis of scatter characteristics, and 10,000 events were acquired per sample. The mean linear units on the forward scatter channel were used as indicators of cell size. CD3⁺ve T cells that did not express CD4 or CD8, were classified as double negative (DN) T cells. Cell sorting was conducted using a FACStar[™] machine (Becton Dickinson). B1a (B220^{int}, CD23^{lo}, CD5⁺ve) or B2 cells (B220^{hi}, CD23^{hi}, CD5[–]ve) were sorted after staining for B220, CD23, and CD5. Sorted cells were typically >95% pure.

ELISA for Total Ig. Total serum IgM and IgG levels were assayed using a sandwich ELISA. In brief, goat anti-mouse IgM or IgG (Boehringer Mannheim) was first coated onto Immulon I plates and blocked. Sera was diluted serially and added to the plates for 2 h at room temperature. Bound Ig was revealed with alkaline-phosphatase conjugated goat anti-mouse IgM or IgG Abs (Boehringer Mannheim), using pNPP as a substrate. Serial dilutions of isotype-specific Ig standards were also added to each plate, for quantitation and interplate standardization.

ELISA for Autoantibodies. The anti-dsDNA, anti-histone, and anti-histone/DNA ELISAs were performed as described previously (21). For the anti-dsDNA ELISA, Immulon II plates (Dynatech) precoated with methylated BSA (mBSA), were coated overnight with 50 ug/ml dsDNA (Sigma-Aldrich, dissolved in PBS, and filtered through cellulose acetate before use). For the anti-histone/DNA ELISA, the dsDNA-coated plates were then postcoated with 10 ug/ml of “total” histones (a mixture of all histones, purchased from Boehringer Mannheim) overnight at 4°C. After blocking with PBS/3% BSA/0.1% gelatin/3 mM EDTA, 1:100 (starting) dilutions of the test-sera, or 1:2 dilutions of culture supernatants, were incubated in duplicate for 2 h at room temperature. Bound IgG was detected with alkaline phosphatase-conjugated anti-mouse IgG (Jackson Immunoresearch Laboratory), using pNPP as a substrate. Raw optical density was converted to U/ml, using a positive control mAb derived from an NZM2410 mouse, arbitrarily setting the reactivity of a 1:100 dilution of this serum to 100 U/ml. This control mAb showed equally strong (OD) reactivities to dsDNA and histone/DNA. Sera with reactivities stronger than the test standard were diluted further and reassayed. The glomerular-binding ELISA was performed as described previously (10), using sonicated rat glomeruli as substrate.

Histopathology. Mice were killed at 3 or 6 mo of age (or earlier, if evidently in distress), and kidneys, spleens, and other internal organs were fixed, sectioned, and stained with H&E, and periodic acid Schiff. For the analysis of kidney sections, at least 100 glomeruli were examined per section, by light microscopy, for evidence of inflammation, and/or tissue damage, as described previously (22), in a blinded fashion. In brief, the severity of GN was graded on 0 to 4 scale, in which the grades 1, 2, 3, and 4, were accorded when 1–10%, 11–25%, 26–50%, and >50% of the glomeruli were affected, respectively. GN of grades 3–4 is referred to in this communication as “severe GN.” The occurrence of any mesangiopathic, capillary hyaline, proliferative, membranous, or crescentic, glomerular changes was also noted. In addition, kidneys were also tested for evidence of Ig deposits by indirect immunofluorescence. Spleens and nodes were examined for their architecture, and any evidence of atypical hyperplasia, lymphomas, etc. In addition, the lungs, hearts, thymus, alimentary tracts, salivary glands, pancreas, liver, and skin of these mice were also sectioned, stained with H&E, and screened for any evidence of pathology.

Clinical Nephritis. Mice were monitored at 3 and 6 mo of age for evidence of clinical nephritis. The total amount of urinary protein was assayed using metabolic cages for urine collection, and a Coomassie-based assay (Pierce Chemical Co.). Typically, normal B6 mice do not excrete >1 mg urinary protein per day.

In addition the levels of blood urea nitrogen (BUN) were measured using a commercially available kit (Sigma-Aldrich). Typically, normal B6 mice do not exhibit >30 mg/dl BUN.

Statistics. Where the samples studied were normally distributed, statistical comparisons were performed using the Student’s *t* test. Where the samples deviated from normality, a nonparametric, Mann Whitney Rank-Sum test was used for comparisons. Statistical analyses were performed using SigmaStat software. For all experiments, the mean and the SEM are also depicted.

Results

B6.Sle1|lpr Mice Exhibit Lymphosplenomegaly, with Altered Lymphocyte Subsets. One of the earliest and most impressive phenotypes that is apparent in B6.Sle1|lpr mice is the massive lymphadenopathy and splenomegaly, evident as early as 2–3 mo of age, as illustrated in Fig. 1. At the age of 3 mo, B6.Sle1|lpr mice (*n* = 6) have mean spleen weights of 413 mg, which are significantly heavier than age-matched B6 (mean = 74 mg, *n* = 8, *P* < 0.002), B6.Sle1 (mean = 90 mg, *n* = 6, *P* < 0.001), and B6.lpr (mean = 105 mg, *n* = 6, *P* < 0.006), as summarized in Table I. Likewise, all LN in this strain are also enlarged. For in-

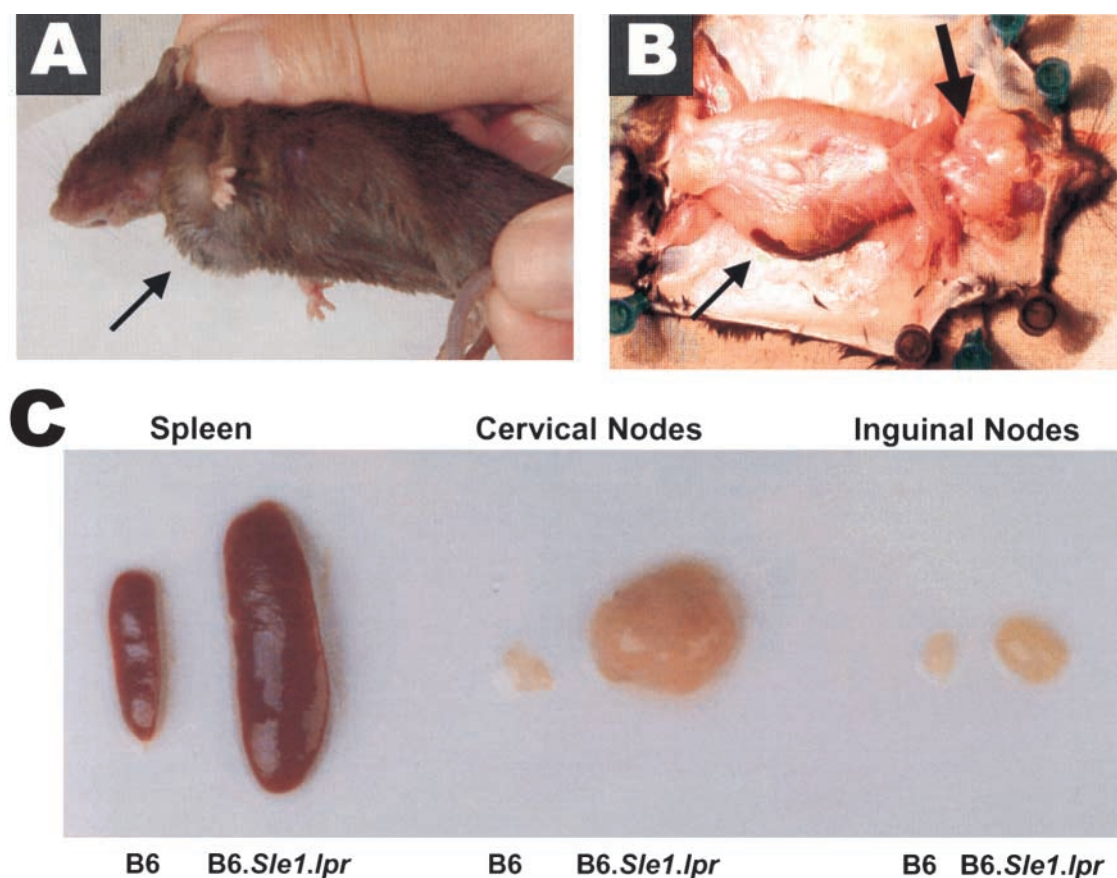


Figure 1. B6.Sle1|lpr mice exhibit prominent splenomegaly and lymphadenopathy, as early as 3 mo of age. (A) The enlarged cervical LNs are visible superficially as early as 3 mo of age. (B) The cervical LNs are grossly enlarged and matted together, abutting onto the submandibular glands. Shown pictures are representative of at least 12 B6.Sle1|lpr mice, at the age of 3 mo. (C) In addition to the cervical LNs, the spleen and inguinal LNs are also enlarged (see Table I for quantitation and statistical analysis). The histology of these enlarged organs are depicted in Fig. 8.

stance, B6.*Sle1*|*lpr* inguinal LNs are ~10-fold larger than the LNs from age-matched controls (Table I).

Evidently, the increased size of the secondary lymphoid organs is partly due to the increased cell numbers, and

partly due to the increased size of individual lymphocytes. In particular, B6.*Sle1*|*lpr* spleens exhibit significantly higher numbers of CD4⁺, and CD4⁻CD8⁻ DN, but not CD8⁺, T cells. On the average, each B6.*Sle1*|*lpr* spleen

Table I. FACS® Analysis of 3-mo-old (mean ± SEM)

| | | B6 | B6. <i>Sle1</i> | B6. <i>lpr</i> | B6. <i>Sle1.lpr</i> | P value ^a | | |
|-------------------------|---|-------------|-----------------|----------------|---------------------|----------------------|-----------------|----------------|
| | | n = 8 | n = 6 | n = 6 | n = 6 | B6 | B6. <i>Sle1</i> | B6. <i>lpr</i> |
| Spleen | Weight (mg) | 74.2 ± 10.6 | 89.6 ± 5.6 | 105.0 ± 9.3 | 413.2 ± 97.2 | ** | *** | ** |
| | Cell number (× 10 ⁶) | 83.1 ± 13.7 | 107.2 ± 10.1 | 127.2 ± 29.1 | 224.6 ± 21.8 | *** | *** | * |
| | % CD4 T cell | 15.4 ± 1.0 | 15.1 ± 0.8 | 16.7 ± 1.1 | 27.5 ± 0.6 | *** | *** | *** |
| | % CD8 T cell | 10.2 ± 0.7 | 10.9 ± 0.5 | 9.6 ± 1.9 | 6.6 ± 0.6 | * | ** | NS |
| | % CD3 ⁺ CD4 ⁻ CD8 ⁻ (DN) | 4.8 ± 1.1 | 8.2 ± 1.2 | 15.1 ± 2.2 | 15.9 ± 2.1 | *** | * | NS |
| | CD4 T cell: size (mean FSC) | 46.1 ± 0.8 | 45.2 ± 0.9 | 50.2 ± 1.1 | 50.6 ± 1.0 | ** | ** | NS |
| | % CD69 ⁺ | 27.1 ± 1.3 | 27.8 ± 0.6 | 35.1 ± 1.2 | 52.5 ± 4.6 | *** | ** | * |
| | % CD25 ⁺ | 25.4 ± 2.8 | 28.2 ± 0.3 | 24.6 ± 2.0 | 42.4 ± 6.9 | * | NS | NS |
| | % CD62L ^{-ve} | 51.9 ± 3.7 | 44.0 ± 3.8 | 72.2 ± 3.4 | 79.0 ± 0.7 | ** | ** | NS |
| | % CD45RB ^{-ve} | 31.8 ± 4.3 | 38.2 ± 3.3 | 50.5 ± 3.6 | 81.4 ± 1.1 | *** | *** | ** |
| | CD8 T cell: % CD69 ⁺ | 18.8 ± 2.6 | 18.6 ± 1.6 | 17.2 ± 0.5 | 47.5 ± 5.2 | *** | ** | ** |
| | % CD25 ⁺ | 12.1 ± 2.0 | 14.8 ± 2.1 | 15.1 ± 3.9 | 37.0 ± 7.2 | ** | * | NS |
| | % CD62L ^{-ve} | 52.4 ± 3.7 | 34.9 ± 4.5 | 65.6 ± 3.5 | 84.9 ± 2.7 | *** | *** | * |
| | % CD45RB ^{-ve} | 10.6 ± 1.9 | 7.1 ± 0.3 | 20.7 ± 7.4 | 38.9 ± 6.4 | ** | *** | NS |
| | % B1a cells | 4.9 ± 0.8 | 10.0 ± 4.7 | 19.9 ± 3.8 | 23.7 ± 4.0 | *** | *** | * |
| | % B2 cells | 53.8 ± 3.3 | 52.1 ± 2.2 | 33.6 ± 6.8 | 16.8 ± 3.4 | *** | *** | *** |
| | B cell: size (mean FSC) | 46.2 ± 0.8 | 48.2 ± 0.8 | 49.1 ± 0.7 | 51.5 ± 0.7 | ** | * | NS |
| | I-A ^b (MFI) ^b | 1,000 | 1,154 ± 55 | 1,163 ± 53 | 2,735 ± 125 | *** | *** | *** |
| B7-1 (MFI) ^b | 50 | 53.6 ± 9.4 | 57.7 ± 4.3 | 78.2 ± 3.9 | * | * | * | |
| B7-2 (MFI) ^b | 50 | 59.8 ± 5.3 | 74.3 ± 14.6 | 93.0 ± 12.5 | ** | * | NS | |
| CD44 (MFI) ^b | 300 | 303.3 ± 9.5 | 360.9 ± 32.6 | 570.9 ± 61.9 | *** | ** | * | |
| LN ^c | Weight (mg) | 7.5 ± 1.1 | 13.6 ± 2.0 | 14.6 ± 2.8 | 111.0 ± 47.1 | * | ** | ** |
| | Cell number (× 10 ⁶) | 2.7 ± 0.4 | 4.3 ± 1.5 | 4.7 ± 1.2 | 17.3 ± 3.1 | ** | ** | ** |
| | % CD4 T cell | 24.1 ± 2.2 | 22.5 ± 2.3 | 18.7 ± 2.2 | 17.7 ± 1.7 | *** | NS | NS |
| | % CD8 T cell | 21.4 ± 2.0 | 23.4 ± 2.9 | 15.2 ± 2.2 | 8.7 ± 1.3 | *** | ** | * |
| | % CD3 ⁺ CD4 ⁻ CD8 ⁻ (DN) | 10.9 ± 2.9 | 8.6 ± 1.4 | 13.4 ± 1.7 | 27.5 ± 3.2 | ** | *** | * |
| | CD4 T cell (mean FSC) | 46.7 ± 1.7 | 45.4 ± 2.0 | 48.2 ± 1.4 | 52.4 ± 0.8 | * | * | * |
| | CD4 T cell: % CD69 ⁺ | 23.8 ± 2.2 | 21.3 ± 1.2 | 35.0 ± 5.0 | 43.0 ± 2.9 | *** | *** | NS |
| | CD8 T cell: % CD69 ⁺ | 15.2 ± 3.6 | 8.0 ± 1.1 | 23.3 ± 9.2 | 29.2 ± 2.9 | * | *** | NS |
| | % B1a cells | 4.5 ± 0.4 | 4.7 ± 0.8 | 15.5 ± 5.1 | 35.1 ± 4.8 | *** | *** | * |
| | % B2 cells | 34.4 ± 4.0 | 31.0 ± 2.2 | 37.0 ± 7.8 | 15.1 ± 3.2 | ** | ** | NS |
| | B cell size (mean FSC) | 44.7 ± 1.7 | 45.5 ± 1.3 | 48.1 ± 1.3 | 53.5 ± 0.6 | *** | ** | * |
| PerC | % B1a cells | 37.6 ± 1.7 | 34.5 ± 3.4 | 38.1 ± 6.1 | 61.1 ± 4.8 | *** | *** | * |
| | % B2 cells | 61.7 ± 0.8 | 56.4 ± 1.3 | 55.6 ± 5.3 | 22.3 ± 0.9 | *** | *** | ** |

Cellular composition of B6.*Sle1*|*lpr* and control spleens, LNs, and PerC. Six to eight mice of each strain were examined at 3 mo of age. Shown values represent mean ± SEM. For the spleen and LNs, the shown percentages of CD4, CD8, DN, B1a, and B2 cells represent percentages of all lymphocytes, whereas the percentages of B1a and B2 cells in the PerC represent percentages of all PerC B cells.

^aStudent's *t* test was performed to compare all three control strains with B6.*Sle1*|*lpr* mice. For the comparison of LN weights, Mann-Whitney Rank Sum test was employed, as these data sets failed normality tests. *P < 0.05; **P < 0.01; and ***P < 0.001. NS, not significant (P > 0.05).

^bEach FACS® staining experiment was conducted with B6 controls and the experimental strains in parallel. Within each experiment, the level of expression of I-A^b, B7-1, B7-2, and CD44 on B6 B cells was arbitrarily set at 1,000, 50, 50, and 300 MFI units, respectively, by adjusting the fluorescence channel voltage. This facilitated the comparison of staining experiments done on different days. MFI, mean fluorescence intensity.

^cShown data was obtained from individual inguinal LNs isolated from the different strains.

bears $61.3 \pm 6.3 \times 10^6$ CD4 T cells ($n = 6$, aged 3 mo), compared with age-matched B6 ($14.1 \pm 2.5 \times 10^6$, $P < 10^{-5}$), B6.*Sle1* ($16.1 \pm 0.5 \times 10^6$, $P < 0.0002$), and B6.*lpr* ($21.2 \pm 2.2 \times 10^6$, $P < 0.02$) spleens, as can be deduced from Table I. Since the absolute numbers of CD8 T cells are not significantly changed, B6.*Sle1|lpr* spleens also exhibit increased CD4:CD8 ratios (mean of six 3-mo-old mice is 4.17), compared with age-matched B6 (mean = 1.5, $n = 8$, $P < 10^{-6}$), B6.*Sle1* (mean = 1.4, $n = 6$, $P < 10^{-5}$), B6.*lpr* (mean = 1.7, $n = 6$, $P < 0.01$), as can be deduced from Table I. In addition, significantly more B6.*Sle1|lpr* T cells exhibit an activated/memory phenotype, as gauged by the surface levels of CD69, CD25, CD62L, and CD45RB, compared with all three control strains. Nearly twice as many 3-mo-old B6.*Sle1|lpr* splenic CD4 T cells bear CD69, compared with the control strains, with a similar trend being noted for CD25. Also, $\sim 80\%$ of 3-mo-old B6.*Sle1|lpr* CD4⁺ T cells phenotype as CD62L^{-ve} and CD45RB^{lo}, and a similar pattern is seen with B6.*Sle1|lpr* CD8⁺ T cells (Table I). Thus, compared with the control strains, B6.*Sle1|lpr* T cells have undergone a massive shift to an activated/memory phenotype.

The *FAS^{lpr}* defect is well known to expand the numbers of DN T cells, which are CD3⁺ve, but negative for CD4 and CD8. These represent CD8 T cells that have failed to undergo activation induced T cell death, and have subsequently downregulated their surface CD8 (23, 24). As reported by others, B6.*lpr* spleens bear significantly higher levels of DN T cells ($\sim 40\%$ of all T cells), compared with B6 and B6.*Sle1* mice (Table I). This unusual subset of T cells is further expanded in B6.*Sle1|lpr* spleens ($54.1 \pm 7.8 \times 10^6$ cells per spleen, $n = 6$), this being significantly higher than the corresponding numbers in B6 ($11.3 \pm 3.2 \times 10^6$ DN T cells per spleen, $P < 0.0008$) and B6.*Sle1* mice ($16.3 \pm 3.5 \times 10^6$ DN T cells per spleen, $P < 0.008$). Although the numbers of DN T cells in B6.*Sle1|lpr* spleens are ~ 2 – 3 -fold higher than the corresponding numbers in B6.*lpr* ($17.9 \pm 6.5 \times 10^6$), these do not reach

statistical significance, owing perhaps to the large variations from mouse to mouse, within both strains. Fig. 2 illustrates the expansion of these T cell subsets in B6.*Sle1|lpr* mice.

B6.*Sle1|lpr* spleens also show significant changes in the B cell compartment. 3-mo-old B6.*Sle1|lpr* spleens have an average of $41.4 \pm 7.0 \times 10^6$ B2 cells each. This is not significantly different from the absolute numbers of B2 cells in B6, B6.*Sle1*, and B6.*lpr* spleens, as can be deduced from Table I. However, B6.*Sle1|lpr* spleens exhibit significantly elevated numbers of B1 cells, mostly B1a cells, expressing CD5. Thus, the absolute numbers of B1a cells in 3-mo-old B6.*Sle1|lpr* spleens ($62.8 \pm 9.8 \times 10^6$) are significantly higher than in the spleens of B6 ($5.6 \pm 1.9 \times 10^6$, $P < 0.0001$), B6.*Sle1* ($11.1 \pm 5.1 \times 10^6$, $P < 0.003$), and B6.*lpr* ($21.1 \pm 5.1 \times 10^6$, $P < 0.02$). Fig. 2 illustrates the expansion of B1a cells in B6.*Sle1|lpr* mice. All strains exhibited minimal levels of B1b cells. B6.*Sle1|lpr* B2 cells also exhibit several features of being already activated in vivo, as demonstrated by their significantly increased size, and heightened (about twofold) surface levels of I-A^b, CD80, CD86, and CD44, compared with the control strains (Table I). Within the data sets examined, both male and female mice appear to be affected equally, with respect to all of the T and B cell phenotypes detailed in Table I.

Similar patterns are also seen in the LNs. B6.*Sle1|lpr* inguinal LNs are ~ 10 -fold larger, and fourfold more hypercellular than the control LNs (Table I). In particular, DN T cells comprise nearly half the lymphocytes in B6.*Sle1|lpr* LNs. Generalized lymphocyte activation, increased CD4:CD8 ratios, and B1a cell expansion are also seen in B6.*Sle1|lpr* LNs (Table I). In the PerC, the combined action of *Sle1* and *FAS^{lpr}* leads to a significant expansion of B1a cells, accounting for nearly two-thirds of all the B cells at this site (Table I). Of note, B1b (B220^{int}, CD23^{lo}, CD5^{-ve}) cells are not prominently expanded in any of the secondary lymphoid organs of the study strains. Finally, similar changes are also noted in the peripheral blood of these mice

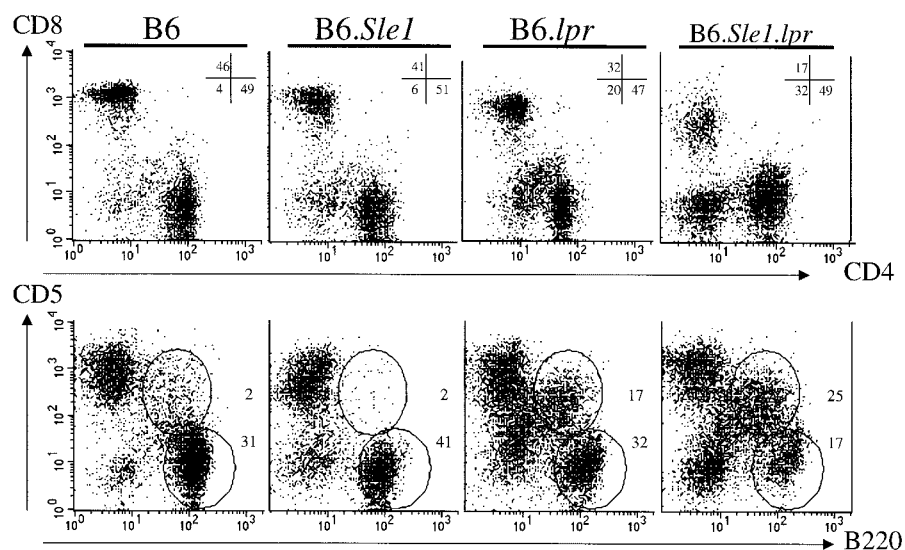


Figure 2. Expansion of unusual subsets of B and T cells in B6.*Sle1|lpr* spleens. Splenocytes from 3-mo-old B6, B6.*Sle1*, B6.*lpr*, and B6.*Sle1|lpr* mice were subjected to FACS[®] analysis as described in Materials and Methods. CD4 versus CD8 plots, gated on live CD3⁺ve cells (top) and B220 versus CD5 plots, gated on all live cells (bottom) are depicted. Shown also are the percentages of CD3⁺ve cells that were CD4⁺ (bottom right), CD8⁺ (top left), or “DN” (bottom left), and the percentages of all live cells that phenotyped as B1a (B220⁺, CD5⁺ve) or B2 (B220^{hi}, CD5^{-ve}, CD23^{lo}). Shown plots are representative of at least six mice from each strain, as detailed and statistically analyzed in Table I.

(unpublished data). As expected, age tends to accentuate these phenotypes. Thus, 6-mo-old B6.*Sle1*|*lpr* spleens are twice as large (546.8 ± 37.7 mg versus 286 ± 32.5 mg, $n = 6$, $P < 0.002$), compared with 3-mo-old B6.*Sle1*|*lpr* spleens. The activation status of B and T cells also exhibit similar trends of accentuation. However, it should be pointed out that the 6-mo data are likely to be “underestimates,” as $>80\%$ of B6.*Sle1*|*lpr* mice are already dead by this age (see below).

B2 Cells, but not B1a Cells, Are the Dominant Producers of IgG ANAs. Given the prominent changes in the B cell compartment of B6.*Sle1*|*lpr* mice (B1a expansion, and activated B2 cells), we next examined if these B cells might be functionally important for disease. Since both the B6.*Sle1* and B6.*lpr* strains are known to have different spectrum of ANAs, we asked if the B6.*Sle1*|*lpr* splenic B cells secrete any ANAs. As diagramed in Fig. 3, A and B, 3-mo-old B6.*Sle1*|*lpr* splenic B cells secrete more IgG anti-ssDNA ($P < 0.0004$, $P < 0.022$, and $P < 0.005$, respectively), IgG anti-dsDNA ($P < 0.008$, $P < 0.036$, and $P < 0.008$, respectively), IgG anti-histone/DNA ($P < 0.032$, $P < 0.036$, and $P < 0.032$, respectively), and IgG anti-histone ANAs ($P < 0.008$, $P < 0.036$, and $P < 0.008$, respectively), compared with age-matched B6, B6.*Sle1*, and B6.*lpr* splenic B cells. Importantly, these differences become very much more pronounced with age. Thus, 6-mo-old B6.*Sle1*|*lpr* splenic B cells secrete 40–700-fold higher levels of IgG ANAs, compared with splenic B cells from age-matched control mice ($P < 0.001$). Given the observation that B6.*Sle1*|*lpr* spleens have increased numbers B1a cells, and activated B2, we next investigated which of these two populations were actually producing the ANAs. To determine this, B2 and B1a cells were FACS[®]-sorted from 3-mo-old B6.*Sle1*|*lpr* spleens, and cultured in vitro for 5 d, with LPS. As depicted in Fig. 3 C, IgG ANAs arise predominantly from splenic B2 cells, rather than B1a cells.

B6.*Sle1*|*lpr* Mice Exhibit a Wide Spectrum of Serum Autoantibodies. As one might have extrapolated from the above findings, the epistatic interaction of *Sle1* with *FAS*^{*lpr/lpr*} also leads to high titres of serum IgM and IgG autoantibodies, as early as 3 mo of age (Fig. 4). This includes anti-nuclear specificities, as well as Abs that acquire affinity for glomerular antigens. Compared with 3-mo-old B6 mice, B6.*Sle1* mice exhibit ~ 1.5 – 2 -fold higher levels of total IgG ($P < 0.009$); however, this monocongenic strain does not exhibit high levels of ANAs at this early age, but only when much older (7). Compared with 3-mo-old B6 mice, B6.*lpr* sera exhibit 1–3-fold higher levels of total IgG ($P < 0.02$), IgG anti-histone ($P < 0.001$), IgG anti-ssDNA ($P < 0.001$), and several specificities of IgM ANAs. B6.*Sle1*|*lpr* mice, as early as 3 mo of age, exhibit significantly elevated total serum IgM and IgG ($P < 0.001$), and an impressive array of IgG and IgM ANAs, targeting ssDNA, dsDNA, histone/DNA, and histones. In addition to ANAs, it is clear from Fig. 4, that B6.*Sle1*|*lpr* mice also develop significantly (100–1,000-fold) higher levels of IgM and IgG anti-glomerular Abs ($P < 0.001$, compared with the control strains). As noted for the cellular phenotypes, age accentuates

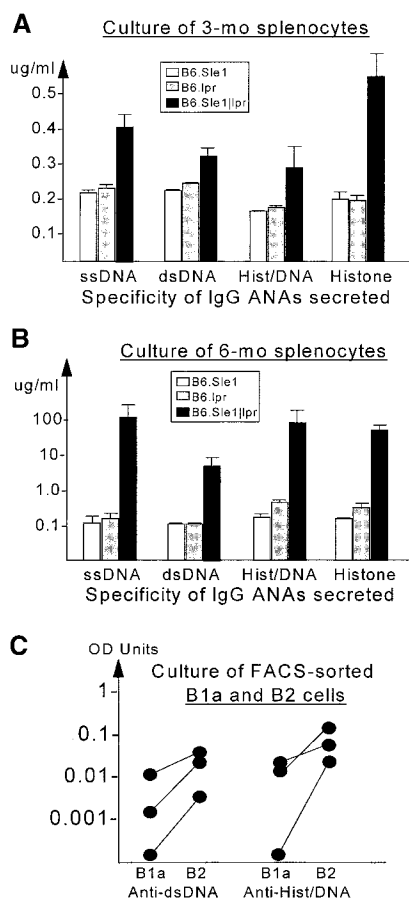


Figure 3. In vitro IgG ANA production of by B6.*Sle1*|*lpr* splenic B cells. Total splenocytes from 3-mo-old (A) and 6-mo-old (B) mice were cultured (10^6 cells per well) for 5 d with LPS. For each strain, splenocytes from 3–6 individual mice were cultured. Shown values represent mean (\pm SEM) levels of ANAs secreted by the 3–6 independent cultures from each strain. B6.*Sle1*|*lpr* splenocytes produce significantly more IgG ANAs, compared with the control strains, both at the 3-mo age ($P < 0.036$), and at the 6-mo age ($P < 0.001$), as detailed in the text. (C) B220^{int}, CD23^{lo}, CD5⁺ (B1a) and B220^{hi}, CD23^{hi}, CD5⁻ (B2) cells were FACS[®] sorted from B6.*Sle1*|*lpr* spleens, and cultured (10^6 cells per well), for 5 d, with LPS. The culture supernatants were assayed for IgG anti-dsDNA and anti-histone/DNA levels, by ELISA. Shown ELISA ODs represent three independent FACS[®] sorting experiments. Within each experiment, the ANA levels produced by B1a cells and B2 cells from the same B6.*Sle1*|*lpr* spleen are shown connected by lines.

ates the ANA serotitres, but the observed levels are likely to be “underestimates,” as $>80\%$ of B6.*Sle1*|*lpr* mice are dead by this age (see below). It is interesting to note that 3-mo-old female B6.*Sle1*|*lpr* mice have significantly higher IgG autoantibody levels to dsDNA ($P < 0.024$), and histone/DNA ($P < 0.026$), and IgM autoantibodies to dsDNA ($P < 0.002$), and ssDNA ($P < 0.008$), compared with their male counterparts (unpublished data). Indeed, this is the only phenotype where we could demonstrate any statistically significant sex differences.

***Sle1* Exerts a Gene-Dosage Effect.** To ascertain the necessity for homozygosity at either of the two loci studied (*Sle1*, *FAS*^{*lpr*}), mice that are heterozygous at these loci were also examined. As depicted in Fig. 5, B6.*Sle1*^{*+/-*}|*lpr*

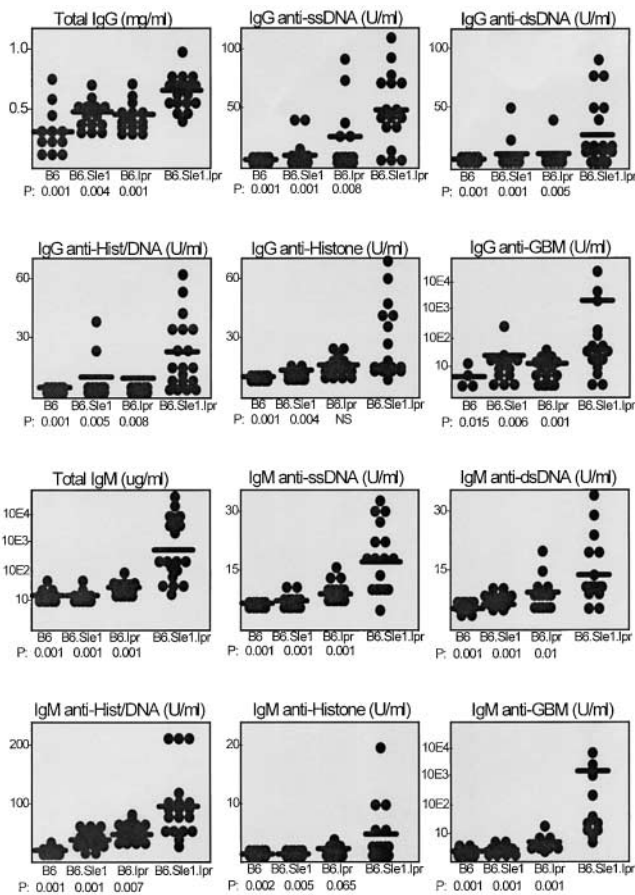
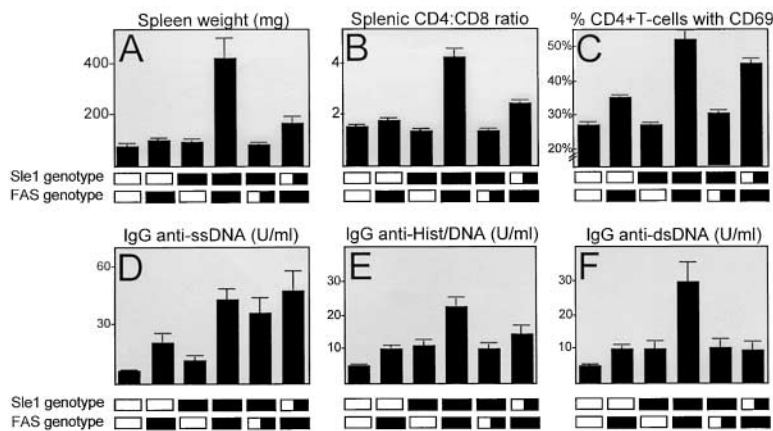


Figure 4. Impact of *Sle1|lpr* on serum Ig and ANAs. 3-mo-old B6 ($n = 14$), B6.*Sle1* ($n = 14$), B6.*lpr* ($n = 6$), and B6.*Sle1|lpr* ($n = 19$) mice were examined for their serum levels of total IgM and IgG, as well as IgM and IgG autoantibodies to ssDNA, dsDNA, histone/DNA, total histones, and renal glomeruli. Sera that exhibited autoantibody levels beyond the linear range of the assay were diluted further, and reassayed. Shown bars depict the mean autoantibody levels in each strain. Depicted below each strain also are the P values, compared with the autoantibody levels in B6.*Sle1|lpr* mice.

mice have significantly larger spleens ($P < 0.025$), increased CD69⁺ CD4 T cells ($P < 0.01$), and elevated serum IgG anti-ssDNA and anti-histone/DNA ANAs ($P < 0.02$), compared with B6.*lpr* mice, as early as 3 mo of age.



However, most of their phenotypes are less dramatic than those seen in B6.*Sle1|lpr* mice. Thus, the B6.*Sle1*^{+/-}*|lpr* spleens weights ($P < 0.02$), CD4:CD8 ratios ($P < 0.004$), mean B cell size ($P < 0.002$), B1a cell expansion ($P < 0.025$), and IgG anti-dsDNA levels ($P < 0.05$), are all significantly less than that seen in B6.*Sle1|lpr* mice (Fig. 5). Thus, in the absence of *FAS* function (*lpr/lpr* genotype), *Sle1* appears to exert a gene dosage effect. In contrast, B6.*Sle1|lpr*^{+/-} mice do not differ significantly from B6.*Sle1* mice, phenotypically. Thus, in the context of the *Sle1/Sle1* genotype, having a single allele of *FAS* negated does not significantly accentuate any of the *Sle1*-triggered phenotypes (Fig. 5).

B6.*Sle1|lpr* Mice Exhibit Severe Clinical and Histological GN. Since the B6.*Sle1|lpr* mice exhibit high titres of potentially pathogenic ANAs, it is important to evaluate the extent of renal pathology and disease in this strain. As depicted in Fig. 6 A, B6.*Sle1|lpr* mice exhibit significantly higher levels of urinary protein, compared with B6 ($P < 0.0003$), and B6.*lpr* mice ($P < 0.02$), as early as 3 mo of age. At this age, B6.*Sle1|lpr* mice also exhibit significantly higher levels of BUN (Fig. 6 B), compared with B6 ($P < 0.001$), B6.*Sle1* ($P < 0.025$), and B6.*lpr* ($P < 0.024$). Both, male and female B6.*Sle1|lpr* mice show equally high 24-h urinary protein ($P = 0.37$) and BUN ($P = 0.24$). Interestingly, there was also a fairly good correlation between IgG anti-dsDNA levels and 24-h urinary protein ($n = 12$ mice, aged 6 mo, correlation coefficient = 0.86). As one would predict, B6.*Sle1|lpr* kidneys demonstrate several features of chronic GN, which become more pronounced with age. These include Grade 4 proliferative glomerulopathy (noted in four out of six kidney sections examined) with hyaline mesangial deposits, evidence of interstitial infiltrates, (as illustrated in Fig. 6 C), pertacious deposits in the tubules, and glomerular Ig deposits (unpublished data). However, no significant vasculitis or tubular changes were seen.

B6.*Sle1|lpr* Mice Exhibit Accelerated Mortality, most likely from Renal Failure. As one might have predicted from the serology and pathology, B6.*Sle1|lpr* mice suffer significantly increased mortality, as diagramed in Fig. 7. At 3 mo of age, none of the B6, B6.*Sle1*, and B6.*lpr* mice are dead,

Figure 5. Impact of heterozygosity at the *Sle1* locus, on autoimmune phenotypes. 3-mo-old B6.*Sle1*^{+/-}*|lpr* mice (heterozygous at *Sle1*, homozygous for *FAS*^{pr}, $n = 6-8$), and B6.*Sle1|lpr*^{+/-} mice (homozygous at *Sle1*, but heterozygous for *FAS*^{pr}, $n = 6-12$), are compared with age-matched B6, B6.*Sle1*, B6.*lpr*, and B6.*Sle1|lpr* mice, with respect to spleen weights (A), splenic CD4:CD8 ratios (B), activation status of splenic CD4 T cells (C), serum IgG anti-ssDNA (D), IgG anti-histone/DNA (E), and IgG anti-dsDNA ANAs (F). Mean \pm SEM are shown. White boxes represent wild-type (B6) alleles, whereas black boxes represent the (NZM2410-derived) *Sle1*, or the mutant *FAS*^{pr} alleles. Thus, the semiopen boxes represent heterozygosity at the respective loci. The data pertaining to the B6, B6.*Sle1*, B6.*lpr*, and B6.*Sle1|lpr* strains can be surmised from Table I and Fig. 4.

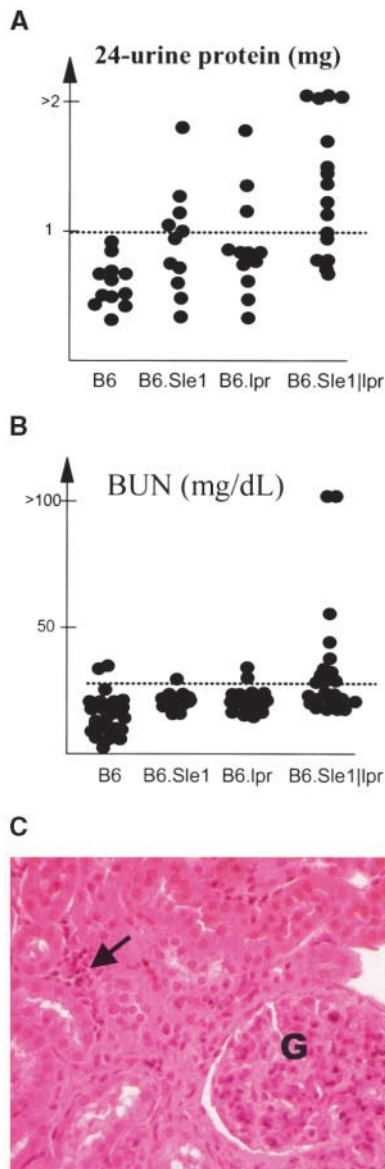


Figure 6. Evidence of renal disease in *B6.Sle1|lpr* mice. (A) BUN and (B) 24-h urinary protein levels were assayed in 3-mo-old B6, *B6.Sle1*, *B6.lpr* and *B6.Sle1|lpr* mice. Each dot represents a single animal. The dotted line represents 2 SD in excess of the mean levels in age-matched B6, which was used as the cut-off to define positives. (C) Typical renal changes included enlarged glomeruli (G) with proliferative changes affecting >50% of glomeruli (Grade 4 GN), and hyaline, mesangial deposits. In addition, two of the six kidneys studied also demonstrated interstitial infiltrates (pointed by arrow).

whereas ~14% of male *B6.Sle1|lpr*, and 28% of female *B6.Sle1|lpr* mice are dead by this age. The cumulative 6-mo mortality rate in this strain is 70% among males, and 90% among females. Although the females tend to have worse mortality, the observed differences are not statistically different. Although these mice have clear evidence of clinical GN (with raised BUN, and increased proteinuria), we wondered if additional pathology elsewhere might also be contributing to death.

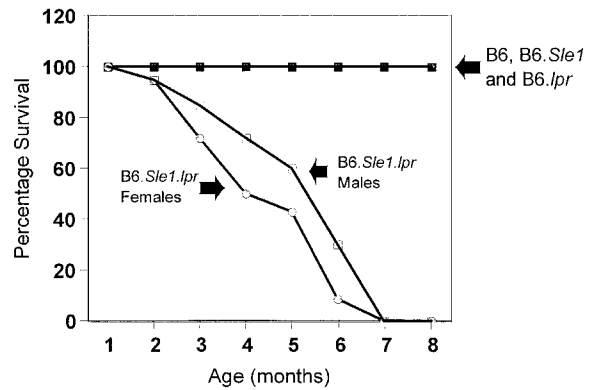


Figure 7. Increased mortality in *B6.Sle1|lpr* mice. A cohort of 16–20 B6, *B6.Sle1*, *B6.lpr*, and *B6.Sle1|lpr* mice were monitored until the age of 8 mo. The three control strains do not exhibit any death until 8 mo of age (solid line, superimposed for all three strains). The mortality curves for the male and female *B6.Sle1|lpr* mice are indicated by dotted lines, as pointed out in the figure.

To explore this, a whole body pathological screen was conducted in 6-mo-old *B6.Sle1|lpr* mice ($n = 5-6$). As expected, *B6.Sle1|lpr* spleens exhibit grossly enlarged white pulp, filled with a sea of reactive lymphocytes (Fig. 8 A). Enlarged reactive LNs (cervical, submandibular, inguinal, pancreatic, and Peyer's patches) were seen in all six of the mice examined. Typically, the medullary sinuses and lymphatic channels of the LNs were plugged with lymphocytes. Some LNs also revealed rich aggregates of plasma cells in the marginal zones. In addition, three out of the six cervical LNs examined revealed areas of hemorrhage (Fig. 8 B). Four out of the five lungs examined, exhibited an angiocentric (but not peribronchial) pattern of cellular infiltrates, as depicted in Fig. 8 C. Five out of six livers examined, exhibited varying degrees of portal triaditis (Fig. 8 D) and nodular hyperplasia (with disarrayed hepatocyte architecture). However, these changes appear unlikely to have caused death in these mice. No significant pathological changes were noted in *B6.Sle1|lpr* heart, skin, thymus, pancreas, salivary gland, stomach, and intestinal sections.

Discussion

We have recently reported that the epistatic interaction of the lupus susceptibility loci, *Sle1* and *Sle3* (on the B6 background), is sufficient to recreate most of the lupus phenotypes seen in lupus-prone NZM2410 mice, from which strain these loci originate (10). Whereas *Sle1* appears to be critical in breaching tolerance to chromatin, *Sle3* reduces activation induced T cell death, accompanied by increased CD4:CD8 ratios, and low titres of ANAs. Indeed, in several respects, *B6.Sle3* mice resemble *B6.lpr* mice, phenotypically (9). Thus, we reasoned that epistatic interactions of *Sle1* with *FAS^{lpr}* mice might also lead to phenotypes that are similar to those seen in *B6.Sle1|Sle3* mice.

As predicted, the epistatic interaction of *Sle1* with *FAS^{lpr}* precipitates several autoimmune features with a

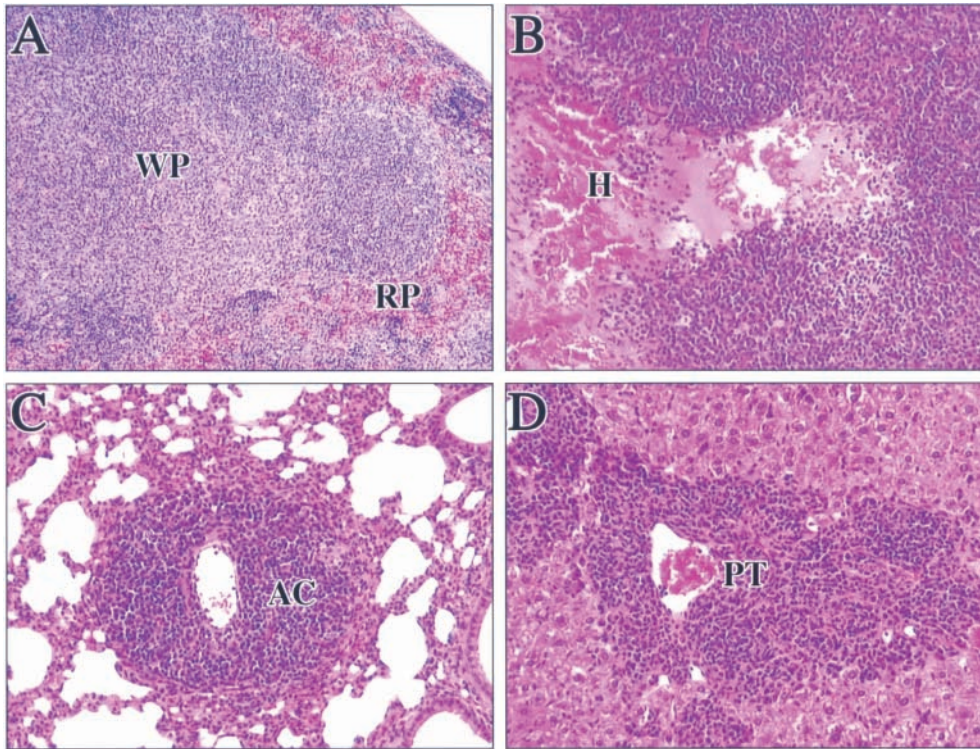


Figure 8. Histopathological changes in other B6.*Sle1|lpr* organs. (A) Spleens, (B) LNs, (C) lungs, and livers of 6-mo-old B6.*Sle1.lpr* ($n = 5-6$) were stained with H&E, and examined for evidence of any pathological changes. B6.*Sle1|lpr* spleens (A) exhibit expansion of the white pulp (WP), compared with the red pulp (RP). The white pulp is expanded by reactive lymphocytes. Shown section is representative of five out of six spleens examined. Similar changes are also seen in the enlarged cervical LNs (B), which are also characterized by areas of hemorrhage (H). Four out of five B6.*Sle1|lpr* lungs (C) demonstrate cellular infiltrates that are curiously localized in an angiocentric fashion (AC), around blood vessels. Five out of six B6.*Sle1|lpr* livers (D) demonstrate cellular infiltrates that showed a congregation around the portal triads (PT), with varying degrees of nodular hyperplasia. Original magnification = $\times 400$.

very early age of onset. The extent of splenomegaly and generalized lymphadenopathy, the degree of lymphocyte activation, the levels of serum ANAs, and the extent of renal disease are far more severe and acute in onset, compared with the B6.*Sle1|Sle3* bicongenic strain (10). Indeed, in many respects, these mice resemble PTEN haploinsufficient mice (25–27). The expansion in absolute numbers of activated CD4⁺ T cells and B cells is remarkable. The increased CD4:CD8 ratios in B6.*Sle1|lpr* mice are similar to those seen in the NZM2410 lupus prone mice. However, the expansion of DN T cells is not a feature of the NZM2410 strain, or the B6.*Sle* congenics. It is very likely that the DN T cells have arisen from CD8⁺ T cells that have failed to undergo apoptosis, as has been demonstrated in B6.*lpr* mice (23, 24). The expansion of DN T cells in B6.*Sle1|lpr* mice (relative to the levels seen in B6.*lpr* mice) suggests that *Sle1* itself is facilitating the activation of CD8 (and CD4) T cells, that then resist AICD, hence leading to an accumulation of these cells as DN T cells. These observations strongly suggest that *Sle1* is also impacting the T cell compartment, in addition to the previously documented intrinsic impact on B cells (12).

B1a cells are not prominent in B6.*Sle1* mice (7). It has also been reported that this population of B cells is not prominent in MRL.*lpr* mice, as well (28). However, in our colony, B6.*lpr* mice themselves reveal a respectable expansion of B1a cells, constituting $\sim 37\%$ of all splenic B-cells, as presented in Table I. In contrast, the epistatic interaction of *Sle1* and *FAS^{lpr}* leads to a massive expansion of B1a cells, which comprise $\sim 60\%$ of splenic B cells in these mice (Table I). The finding that the CD5 molecule be-

comes expressed on anti-self B-cells entering an anergic state after chronic antigenic stimulation (29), and the reports that CD5 transmits inhibitory signals in B cells (30), are consistent with the following model. The epistatic interaction of *Sle1* with *FAS^{lpr}* is sufficient to impede lymphocyte apoptosis strongly enough, so that activated B2 cells accumulate over time. The ongoing incessant autoimmune signaling then drives more and more of these B cells to express CD5, in an “attempt” to downregulate the autoimmune response. Consistent with this model, and the reports from other lupus strains (31–33), most of the IgG ANAs appear to be produced by the B2 cells, rather than the B1a cells (Fig. 2 C). Finally, it is tempting to draw a parallel between the DN T cells and the B1a cells, in these mice: both are believed to represent lymphocytes that have been chronically activated, but had resisted subsequent purging. It is interesting to note that both these unusual populations of lymphocytes are somewhat elevated in B6.*lpr* mice, and both become significantly expanded in B6.*Sle1|lpr* mice.

The serological and renal phenotypes in B6.*Sle1|lpr* mice resemble those seen in B6.*Sle1|Sle2|Sle3* (13), NZM2410, and other lupus models, and do not appear to be unique in any fashion. However, it’s worth stressing the point that the epistatic interaction of *Sle1* and *FAS^{lpr}* is sufficient to engender nephrophilic, anti-dsDNA ANAs, and grade 4 GN with increased proteinuria and BUN, all being phenotypes not prominent in either the B6.*Sle1* or B6.*lpr* strain. Thus, it appears that whereas *Sle1* by itself is sufficient to breach the tolerance of anti-histone/DNA B-cells, the combined defects of *Sle1* and *FAS^{lpr}* are potent enough

to rescue even the nephrophilic and dsDNA-reactive B cells from the tolerance checkpoints. These conclusions are presently being verified using Ig Tg models of tolerance. It is also important to note the fairly good correlation between these phenotypes: the correlation coefficient between IgG anti-dsDNA ANAs and 24-h urinary protein in 6-month-old B6.*Sle1*|*lpr* mice was 0.86. The mortality rate in this strain parallels that in the B6.*Sle1*|*Sle2*|*Sle3* triple congenic mice (13), and is far quicker than in NZM2410 mice. Given the absence of other potential causes of death (based on the pathological survey), and the clear evidence of histological and clinical nephritis, it appears most likely these mice are dying from renal failure.

There are several literature reports of mouse strains with lymphoproliferative autoimmunity on the normal (B6 or B6/129) background with phenotypes close to those seen in B6.*Sle*|*lpr* strain. B6.*lpr*|*Bcl2*^{Tg} mice also develop massive lymphadenopathy with increased numbers of DN T cells (34). However, these mice do not exhibit elevated IgG ANAs, B1 cells, GN, or early mortality. Thus, this strain is clearly different from B6.*Sle1*|*lpr* mice, except for the massive lymphadenopathy. Perhaps the closest resemblance to our strain is the B6/129.*PTEN*^{+/-} strain (25). *PTEN* encodes a phosphatase that is homozygously mutated in a high percentage of human tumors (35, 36). Although homozygous deficiency leads to embryonic lethality, B6/129.*PTEN*^{+/-} mice develop severe lymphadenopathy prominently affecting the submandibular, axillary, and inguinal LNs, similar to B6.*Sle1*|*lpr* mice. These mice also develop high titres of IgG ANAs, and die of GN with a time course that is similar to B6.*Sle1*|*lpr* mice. Importantly, B6/129.*PTEN*^{+/-} mice also exhibit an expanded B1a cell population (25), akin to that observed in the B6.*Sle1*|*lpr* strain. Likewise, mice that hyperexpress PI3 kinase also exhibit similar phenotypes (37). Ongoing studies are aimed at determining how *FAS*^{lpr} and *Sle1* may be differentially impacting specific apoptotic/survival pathways. Collectively, the above reports establish that the infringement of key apoptotic/survival pathways has the potential to trigger lymphoproliferative autoimmunity (38–40).

These studies also have important implications for our understanding of autoimmune lymphoproliferative syndrome (ALPS). Patients with ALPS also develop massive lymphosplenomegaly with concomitant autoimmunity. As extensively reviewed (41–44), most of these patients exhibit mutations in *FAS*/*FASL*. Nevertheless, family studies clearly indicate that *FAS*/*FASL* defects alone may not be sufficient for ALPS to develop – a “second hit” appears to be required (45, 46). Based on the findings in B6.*Sle1*|*lpr* mice, we posit that *Sle1* (and other players in the same pathway) might constitute this “second hit.” It is now clear that *Sle1* is not only a murine lupus/ALPS susceptibility locus, the syntenic region on human chromosome 1 also appears to confer lupus susceptibility (47–49). Thus, this locus on human and murine chromosome 1 potentially holds important clues for our understanding of not only lupus, but also ALPS. Decoding *Sle1* and defining the molecular pathways impacted by *FAS* and *Sle1*

will lay out the molecular blueprints for lymphoproliferative lupus.

We would like to thank Drs. Edward Wakeland and Dwaine Thiele for helpful discussions.

Work in the author’s laboratory is funded by grants from the National Institutes of Health (AR44894 and AI47460) and the Arthritis Foundation. C. Mohan a recipient of the Robert Wood Johnson Jr. Arthritis Investigator Award.

Submitted: 6 June 2001

Revised: 4 April 2002

Accepted: 22 May 2002

References

- Mohan, C. 2001. Murine lupus genetics: lessons learned. *Curr. Opin. Rheumatol.* 13:352–360.
- Kono, D.H., and A.N. Theofilopoulos. 2000. Genetics of systemic autoimmunity in mouse models of lupus. *Int. Rev. Immunol.* 19:367–387.
- Morel, L., U.H. Rudofsky, J.A. Longmate, J. Schiffenbauer, and E.K. Wakeland. 1994. Polygenic control of susceptibility to murine systemic lupus erythematosus. *Immunity.* 1:219–229.
- Morel, L., Y. Yu, K.R. Blenman, R.A. Caldwell, and E.K. Wakeland. 1996. Production of congenic mouse strains carrying genomic intervals containing SLE-susceptibility genes derived from the SLE-prone NZM2410 strain. *Mamm. Genome.* 7:335–339.
- Morel, L., C. Mohan, Y. Yu, B. Croker, X.-H. Tian, A. Deng, and E.K. Wakeland. 1997. Functional dissection of SLE pathogenesis using congenic mouse strains. *J. Immunol.* 158:6019–6028.
- Mohan, C., L. Morel, B. Croker, P. Yang, and E.K. Wakeland. 1997. Genetic dissection of SLE pathogenesis: *Sle2* on murine chromosome 4 leads to B-cell hyperactivity. *J. Immunol.* 159:454–465.
- Mohan, C., E. Alas, L. Morel, P. Yang, and E.K. Wakeland. 1998. Genetic dissection of SLE pathogenesis. *Sle1* on murine chromosome 1 leads to a selective loss of tolerance to H2A/H2B/DNA subnucleosomes. *J. Clin. Invest.* 101:1362–1372.
- Mohan, C., L. Morel, P. Yang, and E.K. Wakeland. 1998. Accumulation of splenic B1a cells with potent antigen-presenting capability in NZM2410 lupus-prone mice. *Arthr. Rheum.* 41:1652–1662.
- Mohan, C., Y. Yu, L. Morel, P. Yang, and E.K. Wakeland. 1999. Genetic dissection of SLE pathogenesis: *Sle3* on murine chromosome 7 impacts T cell activation, differentiation and cell death. *J. Immunol.* 162:6492–6502.
- Mohan, C., L. Morel, P. Yang, H. Watanabe, B. Croker, G. Gilkeson, and E.K. Wakeland. 1999. Genetic dissection of lupus pathogenesis: a recipe for nephrophilic autoantibodies. *J. Clin. Invest.* 103:1685–1695.
- Mohan, C., L. Morel, and E.K. Wakeland. 1999. Genetic insights into murine lupus. In *Lupus. Molecular and Cellular Pathogenesis.* G.M. Kammer and G.C. Tsokos, editors. Humana Press, Totowa, NJ. pp. 124–139.
- Sobel, E.S., C. Mohan, L. Morel, J. Schiffenbauer, and E.K. Wakeland. 1999. Genetic dissection of SLE pathogenesis: adoptive transfer of *Sle1* mediates the loss of tolerance by bone marrow-derived B cells. *J. Immunol.* 162:2415–2421.

13. Morel, L., B.P. Croker, K.R. Blenman, C. Mohan, G. Huang, G. Gilkeson, and E.K. Wakeland. 2000. Genetic reconstitution of systemic lupus erythematosus immunopathology with polycongenic murine strains. *Proc. Natl. Acad. Sci. USA*. 97:6670–6675.
14. Burlingame, R.W., M.A. Volzer, J. Harris, and T.W. Du Clos. 1996. The effect of acute phase proteins on clearance of chromatin from the circulation of normal mice. *J. Immunol.* 156:4783–4788.
15. Burlingame, R.W., M.L. Boey, G. Starkebaum, and R.L. Rubin. 1994. The central role of chromatin in autoimmune responses to histones and DNA in systemic lupus erythematosus. *J. Clin. Invest.* 94:184–192.
16. Amoura, Z., H. Chabre, S. Koutouzov, C. Lotton, A. Cabrespines, J.F. Bach, and L. Jacob. 1994. Nucleosome-restricted antibodies are detected before anti-dsDNA and/or antihistone antibodies in serum of MRL-Mp lpr/lpr and +/+ mice, and are present in kidney eluates of lupus mice with proteinuria. *Arthr. Rheum.* 37:1684–1688.
17. Rubin, R.L., S.A. Bell, and R.W. Burlingame. 1992. Autoantibodies associated with lupus induced by diverse drugs target a similar epitope in the (H2A-H2B)-DNA complex. *J. Clin. Invest.* 90:165–173.
18. Cohen, P.L., and R.A. Eisenberg. 1991. *Lpr* and *gld*: single gene models of systemic autoimmunity and lymphoproliferative disease. *Annu. Rev. Immunol.* 9:269.
19. Izui, S., V.E. Kelley, K. Masuda, H. Yoshida, J.B. Roths, and E.D. Murphy. 1984. Induction of various autoantibodies by mutant gene *lpr* in several strains of mice. *J. Immunol.* 133:227–233.
20. Mixter, P.F., J.Q. Russell, F.H. Durie, and R.C. Budd. 1995. Decreased CD4⁺CD8⁻ TCR- $\alpha\beta$ ⁺ cells in *lpr/lpr* mice lacking β 2-microglobulin. *J. Immunol.* 154:2063–2074.
21. Mohan, C., S. Adams, V. Stanik, and S.K. Datta. 1993. Nucleosome: a major immunogen for pathogenic autoantibody-inducing T cells of lupus. *J. Exp. Med.* 177:1367–1381.
22. Pirani, C.L., and B. Croker. 1994. Handling and processing of renal biopsy and nephrectomy specimens. In *Renal Pathology: With Clinical and Functional Correlations*. C.C. Tisher and B.M. Brenner, editors. J.B. Lippincott Company, Philadelphia. pp. 1683–1694.
23. Pestano, G.A., Y. Zhou, L.A. Trimble, J. Daley, G.F. Weber, and H. Cantor. 1999. Inactivation of misselected CD8 T cells by CD8 gene methylation and cell death. *Science*. 284:1187–1191.
24. Mehal, W.Z., and I.N. Crispe. 1998. TCR ligation on CD8⁺ T cells creates double-negative cells in vivo. *J. Immunol.* 161:1686–1693.
25. Di Cristofano, A., P. Kotsi, Y.F. Peng, C. Cordon-Cardo, K.B. Elkon, and P.P. Pandolfi. 1999. Impaired Fas response and autoimmunity in *Pten*^{+/-} mice. *Science*. 285:2122–2125.
26. Stambolic, V., A. Suzuki, J.L. de la Pompa, G.M. Brothers, C. Mirtsos, T. Sasaki, J. Ruland, J.M. Penninger, D.P. Sidnerovski, and T.W. Mak. 1998. Negative regulation of PKB/Akt-dependent cell survival by the tumor suppressor PTEN. *Cell*. 95:29–39.
27. Cantley, L.C., and B.G. Neel. 1999. New insights into tumor suppression: PTEN suppresses tumor formation by restraining the phosphoinositide 3-kinase/AKT pathway. *Proc. Natl. Acad. Sci. USA*. 96:4240–4245.
28. Bond, A., F.C. Hay, and A. Cooke. 1988. The relationship between induced and spontaneous autoantibodies in MRL mice: the role of Ly-1 B cells? *Immunology*. 64:325–329.
29. Hippen, K.L., L.E. Tze, and T.W. Behrens. 2000. CD5 maintains tolerance in anergic B cells. *J. Exp. Med.* 191:883–890.
30. Bikah, G., J. Carey, J.R. Ciallella, A. Tarakhovskiy, and S. Bondada. 1996. CD5-mediated negative regulation of antigen receptor-induced growth signals in B-1 B cells. *Science*. 274:1906–1909.
31. Reap, E.A., E.S. Sobel, P.L. Cohen, and R.A. Eisenberg. 1992. The role of CD5⁺ B cells in the production of autoantibodies in murine systemic lupus erythematosus. *Ann. NY Acad. Sci.* 651:588–590.
32. Reap, E.A., E.S. Sobel, J.C. Jennette, P.L. Cohen, and R.A. Eisenberg. 1993. Conventional B cells, not B1 cells, are the source of autoantibodies in chronic graft-versus-host disease. *J. Immunol.* 151:7316–7323.
33. Reap, E.A., E.S. Sobel, P.L. Cohen, and R.A. Eisenberg. 1993. Conventional B cells, not B-1 cells, are responsible for producing autoantibodies in *lpr* mice. *J. Exp. Med.* 177:69–78.
34. Reap, E.A., N.J. Felix, P.A. Wolthuisen, B.L. Kotzin, P.L. Cohen, and R.A. Eisenberg. 1995. Bcl-2 transgenic *lpr* mice show profound enhancement of lymphadenopathy. *J. Immunol.* 155:5455–5462.
35. Li, J., L. Simpson, M. Takahashi, C. Miliareisis, M.P. Myers, N. Tonks, and R. Parsons. 1998. The PTEN/MMAC1 tumor suppressor induces cell death that is rescued by the AKT/protein kinase B oncogene. *Cancer Res.* 58:5667–5672.
36. Dahia, P.L., R.C. Aguiar, J. Alberta, J.B. Kum, S. Caron, H. Sill, D.J. Marsh, J. Ritz, A. Freedman, C. Stiles, et al. 1999. PTEN is inversely correlated with the cell survival factor Akt/PKB and is inactivated via multiple mechanisms in hematological malignancies. *Human Mol. Gen.* 8:185–193.
37. Borlado, L.R., C. Redondo, B. Alvarez, C. Jimenez, L.M. Criado, J. Flores, M.A. Marcos, A. Martinez, D. Balomenos, and A.C. Carrera. 2000. Increased phosphoinositide 3-kinase activity induces a lymphoproliferative disorder and contributes to tumor generation in vivo. *FASEB J.* 14:895–903.
38. Chervonsky, A.V. 1999. Apoptotic and effector pathways in autoimmunity. *Curr. Opin. Immunol.* 11:684–688.
39. Scaffidi, C., S. Kirchhoff, P.H. Krammer, and M.E. Peter. 1999. Apoptosis signaling in lymphocytes. *Curr. Opin. Immunol.* 11:277–285.
40. Refaelli, Y., L. Van Parijs, and A.K. Abbas. 1999. Genetic models of abnormal apoptosis in lymphocytes. *Immunol. Rev.* 169:273–282.
41. Rieux-Laucat, F., F. Le Deist, C. Hivroz, I.A. Roberts, K. Debatin, A. Fischer, and J.P. deVillantay. 1995. Mutations in Fas associated with human lymphoproliferative syndrome and autoimmunity. *Science*. 268:1347–1349.
42. Drappa, J., A. Vaishnav, K. Sullivan, J. Chu, and K.B. Elkon. 1996. Fas gene mutations in the Canale-Smith syndrome, an inherited lymphoproliferative disorder associated with autoimmunity. *N. Engl. J. Med.* 335:1643–1649.
43. Strauss, S.E., E.S. Jaffe, J.M. Puck, J.K. Dale, K.B. Elkon, A. Rosen-Wolff, A.M. Peters, M.G. Sneller, C.W. Hallahan, J. Wang, et al. 2001. The development of lymphomas in families with autoimmune lymphoproliferative syndrome with germline Fas mutations and defective lymphocyte apoptosis. *Blood*. 98:194–200.
44. Chun, H.J., and M.J. Lenardo. 2001. Autoimmune lymphoproliferative syndrome: types I, II and beyond. *Adv. Exp. Med. Biol.* 490:49–57.
45. Jackson, C., R.E., Fischer, A.P. Hsu, S.M. Anderson, Y.

- Choi, J. Wang, J.K. Sale, T.A. Fleisher, L.A. Middleton, M.C. Sneller, et al. 1999. Autoimmune lymphoproliferative syndrome with defective Fas: genotype influences penetrance. *Am. J. Hum. Genet.* 64:1002–1014.
46. Bleesing, J.J., M.R. Brown, S.E. Straus, J.K. Dale, R.M. Siegel, M. Johnson, M.J. Lenardo, J.M. Puck, and T.A. Fleisher. 2001. Immunophenotypic profiles in families with autoimmune lymphoproliferative syndrome. *Blood.* 98:2466–2473.
47. Kotzin, B.L. 1997. Susceptibility loci for lupus: a guiding light from murine models? *J. Clin. Invest.* 99:557–558.
48. Tsao, B.P., R.M. Cantor, K.L. Kalunian, C.-I. Chen, R. Singh, D.J. Wallace, R.L. Kitridou, S.I. Chen, N. Shen, Y.W. Song, D.A. Isenberg, C.-I. Yu, B.H. Hahn, and J.I. Rotter. 1997. Evidence for linkage of a candidate chromosome 1 region to systemic lupus erythematosus. *J. Clin. Invest.* 99:725–731.
49. Wakeland, E.K., K. Liu, R.R. Graham, and T.W. Behrens. 2001. Delineating the genetic basis of systemic lupus erythematosus. *Immunity.* 15:397–408.